Functional instability allows access to DNA in longer Transcription Activator-Like Effector (TALE) arrays.

Kathryn Geiger-Schuller[1,2], Jaba Mitra[3], Taekjip Ha[1,4,5,6], & Doug Barrick[1]*

[1]T.C. Jenkins Department of Biophysics and Program in Molecular Biophysics, Johns Hopkins University, 3400 N. Charles St, Baltimore MD 21218.

[2]Current address: Broad Institute of Harvard and Massachusetts Institute of Technology, Cambridge, MA 02142.

[3]Materials Science and Engineering, University of Illinois Urbana-Champaign, Urbana IL 61801.

[4]Department of Physics, Center for the Physics of Living Cells and Institute for Genomic Biology, University of Illinois at Urbana Champaign, Urbana IL 61801.

[5]Department of Biophysics and Biophysical Chemistry and Department of Biomedical Engineering, Johns Hopkins University, Baltimore MD 21205.

[6]Howard Hughes Medical Institute, Baltimore, MD, 21205, USA

*Corresponding Author: barrick@jhu.edu, (410) 516-0409

Keywords: TALE repeat, Single-molecule biophysics, FRET, Functional instability, Deterministic modeling

Abstract

Transcription activator-like effectors (TALEs) bind DNA through an array of tandem 34-residue repeats. Here, we examine the kinetics of DNA binding for a set of TALE arrays with varying numbers of identical repeats using single molecule microscopy. Using a new deterministic modeling approach, we find evidence for conformational heterogeneity in both the free- and DNA-bound TALE arrays. Combined with previous work demonstrating populations of partly folded TALE states, our findings reveal a functional instability in TALE-DNA binding. For TALEs forming less than one superhelical turn around DNA, partly folded open states inhibit DNA binding. In contrast, for TALEs forming more than one turn, the partly folded open states facilitate DNA binding. Overall, we find that increasing repeat number results in significantly slower interconversion between the various DNA-free and DNA-bound states. These findings highlight the role of conformational heterogeneity and dynamics in facilitating macromolecular complex assembly.

Impact Statement

Single molecule DNA-binding trajectories and deterministic modeling analyses demonstrate a functional role for high energy partly folded states in Transcription Activator-Like Effectors (TALEs) that could improve future TALEN design.

Introduction

Transcription activator-like effectors (TALEs) are bacterial proteins containing a domain of tandem DNA-binding repeats as well as a eukaryotic transcriptional activation domain (Kay et al., 2007; Römer et al., 2007). The repeat domain binds double stranded DNA with a register of one repeat per base pair. Specificity is determined by the sequence identity at positions twelve and thirteen in each TALE repeat, which are referred to as repeat variable diresidues (RVDs) (Boch et al., 2009; Miller et al., 2015; Moscou and Bogdanove, 2009). This specificity code has enabled design of TALE-based tools for transcriptional control (Cong et al., 2012; Geissler et al., 2011; Li et al., 2012; Mahfouz et al., 2012; Zhang et al., 2011), DNA modifications (Maeder et al., 2013), in-cell microscopy (Ma et al., 2013; Miyanari et al., 2013), and genome editing (TALENs) (Christian et al., 2010; Li et al., 2011).

TALE repeat domains wrap around DNA in a continuous superhelix of 11.5 TALE repeats per turn (Deng et al., 2012; Mak et al., 2012). Because TALEs contain on average 17.5 repeats (Boch and Bonas, 2010), most form over 1.5 full turns around DNA. Many multisubunit proteins that form rings around DNA require energy in the form of ATP to open or close around DNA (reviewed in O'Donnell and Kuriyan, 2006), yet

TALEs are capable of wrapping around DNA without energy from nucleotide triphosphate hydrolysis. One possibility is that TALEs bind DNA through an energetically accessible open conformation. Consistent with this possibility, we previously demonstrated that TALE arrays can populate partly folded or broken states (Geiger-Schuller and Barrick, 2016). While the calculated populations of partly folded states in TALE repeat arrays are small, these populations are many orders of magnitude larger than calculated populations of partly folded states in other previously studied repeat arrays (consensus Ankyrin (Aksel et al., 2011) and DHR proteins (Geiger-Schuller et al., 2018)) suggesting a potential functional role for the high populations of partially folded states in TALE repeat arrays.

Consensus TALEs (cTALEs) are homopolymeric arrays composed of the most commonly observed residue at each of the 34 positions of the repeat (Geiger-Schuller and Barrick, 2016). In addition to simplifying analysis of folding and conformational heterogeneity in this study, the consensus approach simplifies analysis of DNA binding, eliminating contributions from sequence heterogeneity and providing an easy means of site-specific labeling.

Here we characterize DNA binding kinetics of cTALEs using total internal reflection fluorescence single-molecule microscopy. We find that consensus TALE arrays bind to DNA reversibly, with high affinity. Analysis of the dwell-times of the on- and off-states reveals multiphasic binding and unbinding kinetics, suggesting conformational heterogeneity in both the free and DNA bound state. We develop a deterministic optimization analysis that supports such a model, and provides rate

constants for both conformational changes and binding. Comparing the dynamics observed here to previously characterized local unfolding suggests that locally unfolded states inhibit binding of short cTALE arrays (less than one full superhelical turn around DNA), whereas they promote binding of long arrays (more than 1 full superhelical turn). Whereas local folding of transcription factors upon DNA binding is well documented (Spolar and Record, 1994), local unfolding in the binding process has not. Our results present a new mode of transcription factor binding where the major conformer in the unbound state is fully folded, requiring partial unfolding prior to binding. The critical role of such high energy partly folded states is an exciting example of functional instability.

Results

cTALE design

Consensus TALE (cTALE) repeat sequence was design previously described (Geiger-Schuller and Barrick, 2016). To avoid self- association of cTALE arrays, we fused arrays to a conserved N-terminal extension of the PthXo1 gene. Although the sequence of this domain differs from a TALE repeat sequence, the structure of this domain closely mimics four TALE repeats (Gao et al., 2012; Mak et al., 2012) and is required for full transcriptional activation (Gao et al., 2012). In this study, all repeat arrays contain this solubilizing N-terminal domain.

cTALE local instability promotes population of partly folded states

Figure 1A depicts types of partly folded states of a generic repeat protein. In the fully folded state, all repeats are folded, and all interfaces are intact. In the end-frayed states, one or more terminal repeats are unfolded and all interfaces, except the interface(s) between the unfolded and adjacent folded repeat(s), are intact. In the internally unfolded states, a central repeat is unfolded and all interfaces, except the interfaces involving the unfolded repeats, are intact. In the interfacially ruptured state, all repeats are folded but one interface is disrupted due to local structural distortion.

Figure 1B shows calculated free energy differences between various partly folded states and the fully folded repeat array for two different RVDs (NS and HD) in an otherwise identical consensus sequence background, using the intrinsic and interfacial engeries we determined previously (Geiger-Schuller and Barrick, 2016). The distribution of partly folded states is calculated for different 20-repeat arrays containing two types of TALE arrays (with the NS RVD in red and with the HD RVD in blue) as well as consensus ankyrin arrays (cAnk in black). For cTALE arrays, end frayed states are within a few *RT* of the folded state, internally unfolded states are highest in energy, and interfacially ruptured states fall energetically between end frayed and internally unfolded states.

Changing the RVD sequence affects the distribution of these partly folded states: HD repeat containing arrays are more likely to internally unfold or interfacially rupture than NS repeat containing arrays. However, both types of cTALEs are more likely to populate many of these partly folded states than cAnk is to populate even the lowest energy partly folded state, the end frayed state. Thus, compared to ankyrin repeats,

cTALEs are locally unstable, meaning they are likely to form partly folded states. As these states disrupt the superhelix, they may facilitate DNA binding.

Single-molecule studies of cTALE binding to DNA

To ask if cTALE local instability is relevant for DNA binding kinetics, DNA binding trajectories were measured using single molecule total internal reflection fluorescence (smTIRF). Figure 2A shows a schematic of the smTIRF experiments performed to measure DNA binding. For site-specific cTALE labeling, R30 is mutated to cysteine in a single repeat. Position 30 is frequently a cysteine in naturally occurring TALEs (in earlier folding studies, arginine was chosen in the consensus sequence to avoid disulfide formation) (Geiger-Schuller and Barrick, 2016). This cysteine was Cy3 (FRET donor)-labelled using maleimide chemistry, and was attached to biotinylated slides via the C-terminal His_6 tag and α-Penta•His antibodies. At salt concentrations below 300 mM NaCl, cTALEs aggregate. Because DNA binding is weak at high salt concentrations, measuring binding kinetics in bulk at high salt is not possible. However, tethering cTALEs to the quartz slide at high salt prevents self-association, even at the low salt concentrations required to study DNA binding kinetics. A histogram of $NcTALE_8$ (8 NS-type repeats and the N-terminal domain) labeled via a cysteine in the first repeat shows a single peak at zero FRET efficiency, as expected for donor-only constructs (Figure 2B).

To test for DNA binding to tethered cTALE constructs, we added Cy5 (FRET acceptor)-labeled 15 bp-long DNA ($Cy5.A_{15}/T_{15}$) to tethered $NcTALE_8$. This results in a

new peak at a FRET efficiency of 0.45, indicating that DNA binds directly to cTALE arrays. As DNA concentration in solution is increased, the peak at 0.45 FRET efficiency increases in population (Figure 2C-D), suggesting a measurable equilibrium between free and bound DNA rather than saturation or irreversible binding. In support of this, single molecule time trajectories show interconversion between bound and unbound states, providing access to rates of binding and dissociation.

As expected for reversible complex formation, the peak at 0.45 FRET efficiency can be competed away by adding mixtures of labeled and unlabeled DNA to pre-formed cTALE-labelled DNA complexes (schematic shown in Figure 2E; pre-formed complex shown in Figure 2F, competition data shown in Figure 2G-H). Challenging pre-formed complexes with a mixture of 5 nM unlabeled DNA and 15 nM labeled DNA results in a slight decrease in the population of the peak at 0.45 FRET (compare Figures 2F and 2G). Challenging with a mixture of 50 nM unlabeled DNA and 15 nM labeled DNA further decreases the peak at 0.45 FRET (Figure 2H).

cTALE arrays display multiphasic DNA-binding kinetics.

In addition to the short smTIRF movies used to generate smFRET histograms from many molecules, long movies were also collected to examine the extended transitions of individual molecules between the low- and high-FRET (0 and 0.45) (Figure 3A-B). A transition from low to high FRET (0 to 0.45) indicates that the acceptor fluorophore on DNA moved close enough to the donor on the protein for FRET and is likely a binding event. A transition from high to low FRET (0.45 to 0.0) indicates the

169 acceptor fluorophore on DNA moved too far away from the donor on the protein for
170 FRET and is likely an unbinding event. Low-FRET states show low colocalization with
171 signal upon direct excitation of the acceptor, confirming that high-FRET states are DNA-
172 bound states and low-FRET states are DNA-free states (Figure 3- figure supplement 1).
173 These long single molecule traces show both long- and short-lived low- and high-FRET
174 states, indicating that kinetics are multi-phasic (Figure 3A-B). Binding events (transitions
175 from low to high FRET) become more frequent as bulk DNA concentration increases
176 (compare representative traces at 1 nM dsDNA to 15 nM dsDNA; Figure 3A and Figure
177 3B). Cumulative distributions generated from dwell times in the low FRET state at a
178 given DNA concentration are best-fit by a double-exponential decay, indicating a
179 minimum of two kinetic phases associated with binding events (Figure 3C). Cumulative
180 distributions generated from dwell times in the high FRET state are best-fit by a double-
181 exponential decay, indicating that there are a minimum of two kinetic phases for
182 unbinding as well (Figure 3D).

183 The rate constant for the fast phase in DNA binding shows a linear increase with
184 DNA concentration (Figure 3E), indicating that this step involves an associative binding
185 mechanism. The slope of these rate constants as a function of DNA concentration gives
186 a bimolecular rate constant of 5.9×10^8 $nM^{-1}s^{-1}$, close to the diffusion limit. The rate
187 constant for the slower phase (0.59 s^{-1}) is independent of DNA concentration indicating
188 a unimolecular isomerization mechanism (Figure 3E).

189 In contrast, neither of the two fitted rate constants for transitions from high to low
190 FRET (0.45 to 0.0; unbinding events) depends on DNA concentration, suggesting that

unbinding involves two (or more) unimolecular processes (Figure 3F). The rate constants of these two phases are 1.2 s^{-1} and 0.13 s^{-1} respectively.

To rule out kinetic contributions of TALEs threading axially onto the ends of short DNAs, binding kinetics were measured with capped double-helical DNA sites. Capped DNA was generated by forming 5'digoxygenin-A_5-Cy5-A_{15} duplexed with 5'-digoxygenin-T_{26} and adding a three-fold molar excess of anti-Digoxygenin. Low and high FRET dwell time cumulative distributions generated from capped DNA-binding kinetics are bi-phasic, similar to distributions from uncapped DNA (Figure 3- figure supplement 2). The DNA concentration-independent rate constant for binding is roughly the same for capped DNA as for uncapped DNA (compare $FRET_{L\rightarrow H}$ red and blue triangles in Figure 3- figure supplement 2), as are the dissociation rate constants (compare $FRET_{H\rightarrow L}$ red and blue triangles in as well as $FRET_{H\rightarrow L}$ red and blue circles in Figure 3- figure supplement 2). The rate constant for bimolecular binding of capped DNA decreases compared to that for uncapped DNA (compare $FRET_{L\rightarrow H}$ red and blue circles in Figure 3- figure supplement 2), which is consistent with the expected decrease in the rate of diffusion of the larger capped DNA. To assess the effect of molecular weight increase on diffusion of capped versus uncapped DNA, Sednterp (edited by S. E. Harding, 1992), a program commonly used to estimate sedimentation and diffusion properties of biomolecules, was used to estimate maximum diffusion coefficients. Including the two antibodies bound on the ends of capped DNA (320 kDa total) gives an estimated diffusion coefficient of 4.7×10^{-7} cm^2s^{-1}, which is much lower than the estimated diffusion coefficient of the uncapped DNA (1.5×10^{-6} cm^2s^{-1}). This ~3.6-fold decrease in the

diffusion constant for capped DNA is similar to the 6.7-fold decrease in the bimolecular rate constant for binding of capped DNA (Figure 3- figure supplement 2).

Longer cTALEs have slower DNA binding and unbinding kinetics

To examine how increasing the length of the cTALE array influences DNA binding, we generated Cy3-labelled constructs with 16 and 12 cTALE repeats, and measured binding to a longer Cy5-labelled DNA (A_{23}/T_{23}). Because we did not observe FRET for these longer constructs, a fluorescence colocalization microscopy protocol was used instead (Figure 4- figure supplement 1). In this protocol, Cy3 was first imaged for ten camera frames (1017.5 msec total) to identify positions of single TALE molecules. Then a long time series of fluorescence images of Cy5 signal were collected through directly exciting Cy5 on the DNA, and time trajectories of Cy5 signal were generated from the initially identified single TALE positions.

Increasing the number of cTALE repeats from 8 to 12 and 16 dramatically affects DNA binding kinetics. Long movies collected over a range of DNA concentrations show short- and long-lived Cy5 signal on and off states, indicating a level of kinetic heterogeneity similar to $NcTALE_8$ (Figure 4- figure supplement 1). Single molecule traces were analyzed using a thresholding filter (see Materials and Methods and Figure 4- figure supplement 1) to identify states and dwell times. Cumulative distributions were generated from dwell times at low Cy5 signal (unbound states, with lifetimes representing binding kinetics), and at high Cy5 signal (bound states, with dwell times representing unbinding kinetics). As with the eight repeat constructs, unbound

cumulative distributions for these longer TALE arrays are best-fit by double exponential decays, particularly at high DNA concentrations (compare the cumulative distribution at low DNA concentration, Figure 4- figure supplement 2A, to cumulative distribution at 5 nM DNA, Figure 4- figure supplement 2B). Bound cumulative distributions for longer TALE arrays are best-fit by double exponential decays (Figure 4- figure supplement 2C-D). All apparent rate constants are much smaller for $NcTALE_{16}$ and $NcTALE_{12}$ (green/black circles and triangles, Figure 4A-B) compared to $NcTALE_{8}$, indicating that binding and unbinding is impeded by increasing the length of the binding surface between cTALEs and their cognate DNA (Figure 4C). To address whether differences in binding kinetics are related to experimental differences between colocalization and FRET assays, alternating laser experiments were performed by switching between FRET and colocalization detection (every 5 frames) within single molecule trajectories (Figure 3- figure supplement 1). Changes in FRET and colocalization signals occurred simultaneously according to single molecule time traces, showing that differences in binding and unbinding kinetics of short and longer cTALEs are not due to differences in colocalization and FRET assays (Figure 3 - figure supplement 1).

A deterministic approach to modeling cTALE-DNA binding kinetics.

To determine how the kinetic changes above are partitioned into underlying kinetic steps in binding, we fitted various kinetic models to the cumulative distributions for binding and unbinding. In addition to providing information about the mechanism of binding, this approach allows us to estimate the underlying microscopic rate constants

and compare them for different constructs. This approach is generally applicable to studies of complex single molecule kinetics. Numerical integration was used to calculate the relative population of cTALE states as a function of time (Figures 5A-C and 5G-H), given a binding mechanism, an associated set of rate laws, and a set of initial conditions. Cumulative distributions of unbound dwell times represent the distribution of times single molecules spent in the unbound state before transitioning into the bound state, allowing us to split the kinetic scheme when fitting to single-molecule dwell times.

Among the various models tested, the model that is most consistent with the data has two unbound DNA-free states and two DNA-bound states. This is consistent with alternating laser experiments showing that DNA is only colocalized when cTALEs are in the high FRET state (Figure 3 - figure supplement 1). This four-state model includes a TALE isomerization step in the absence of DNA from a DNA-binding incompetent conformation (which we refer to as TALE) to DNA-binding competent conformation (which we refer to as TALE*). The DNA-binding competent TALE* conformer binds and unbinds DNA (called TALE* when DNA free and TALE*~DNA when DNA-bound). Before unbinding, a fraction of TALE*~DNA isomerizes to a longer-lived DNA-bound state called $TALE^{\ddagger}$~DNA.

Based on this mechanism, the rate laws for binding are given in equations 1a - 1d.

$$\frac{d[TALE]}{dt} = -k_1[TALE] + k_{-1}[TALE^*] \quad (1a)$$

$$\frac{d[TALE^*]}{dt} = k_1[TALE] - k_{-1}[TALE^*] - k_2[TALE^*][DNA] \quad (1b)$$

$$\frac{d[TALE^* \sim DNA]}{dt} = k_2[TALE^*][DNA] \quad (1c)$$

$$K_{eq,DNA-free} = \frac{k_1}{k_{-1}} \quad (1d)$$

Since the single-molecule dwell-time histograms of the unbound states are insensitive to the isomerization after DNA binding, the equation describing the time evolution of the long-lived bound state (TALE‡~DNA) is not relevant to our analysis of unbound-state lifetimes.

To determine microscopic rate constants k_1, k_{-1}, and k_2, equations 1a-1c were numerically integrated in Matlab, and the fraction of TALE*~DNA as a function of time was fitted to the low-FRET cumulative distributions (NcTALE$_8$; Figure 5D-E) or to the no colocalization cumulative distributions (NcTALE$_{16}$; Figure 5J-K). Microscopic rate constants were adjusted to reduce sum of the squared residuals between the concentration of TALE*~DNA (the direct product of binding) as a function of time and single-molecule cumulative distributions. In both cases, cumulative distributions at different bulk DNA concentrations were fitted globally. Initial fractions of TALE and TALE*~DNA were set to zero, and the initial fraction of TALE* was set to one. Confidence intervals (CI) were estimated by bootstrapping (Table 1; mean and 68% CI from 2000 or 8000 bootstrap iterations).

Rate laws for dissociation are given in equations 2a - 2d

$$\frac{d[TALE^* \sim DNA]}{dt} = -k_{-2}[TALE^* \sim DNA] - k_3[TALE^* \sim DNA] + k_{-3}[TALE^{\ddagger} \sim DNA] \quad (2a)$$

$$\frac{d[TALE^{\ddagger} \sim DNA]}{dt} = k_3[TALE^* \sim DNA] - k_{-3}[TALE^{\ddagger} \sim DNA] \quad (2b)$$

298 $$\frac{d[TALE^*]}{dt} = k_{-2}[TALE^* \sim DNA] \quad (2c)$$

299 $$K_{eq,DNA-bound} = \frac{k_3}{k_{-3}} \quad (2d)$$

300 As with the system of equations above (1a-d), the equation describing the time
301 evolution of the binding-incompetent free state (TALE) is not relevant to our analysis of
302 bound-state lifetimes.

303 To determine microscopic rate constants k_{-2}, k_{-3}, and k_3, equations 2a-2c were
304 numerically integrated in Matlab, and the fraction of TALE* as a function of time was
305 fitted to the high-FRET cumulative distributions ($NcTALE_8$; Figure 5F) or to the low
306 colocalization cumulative distributions ($NcTALE_{16}$; Figure 5L). Microscopic rate
307 constants were adjusted to reduce sum of the squared residuals between the
308 concentration of TALE* (the direct product of dissociation) as a function of time and
309 single-molecule cumulative distributions. In both cases, cumulative distributions at
310 different bulk DNA concentrations were fitted globally. The initial fraction of
311 TALE*~DNA conformer was set at one; all other initial fractions were set to zero.
312 Confidence intervals were estimated by bootstrapping (Table 1; mean and 68% CI from
313 2000 iterations).

314 Fitted curves reproduce the experimental cumulative distributions for binding and
315 unbinding (Figure 5), both for the short and long cTALE arrays, with reasonably small
316 residuals, over a range of DNA concentrations. Generally, fitted rate constants have
317 confidence intervals of 10% or smaller (Table 1).

Comparison of microscopic rate constants for 8, 12, and 16 repeats show some significant differences. The bimolecular microscopic binding rate constant, k_2, is slightly larger for 8 repeats than for 12 and 16 repeats (1.1, 0.31, and 0.39 $nM^{-1}s^{-1}$ for 8, 12, and 16 repeats respectively). However, microscopic unbinding rate constant, k_{-2}, is higher for 8 repeat cTALEs (0.66 s^{-1} for $NcTALE_8$ versus 0.13 s^{-1} for $NcTALE_{12}$ and 0.299 s^{-1} for $NcTALE_{16}$). Also, bound state isomerization (interconversion between TALE*~DNA and $TALE^{\ddagger}$~DNA) is 5-10 times slower for 16 and 12 repeat cTALEs than 8 repeat cTALEs. The value of $K_{eq,\ DNA\text{-}free}$, which is a measure of the equilibrium proportion of the unbound TALE that is DNA-binding competent (TALE*) to that which is binding-incompetent (TALE), is larger for cTALEs with 8 repeats ($K_{eq,\ DNA\text{-}free} = 1.32$) than for cTALEs with 12 and 16 repeats ($K_{eq,\ DNA\text{-}free} = 0.11$ and $K_{eq,\ DNA\text{-}free} = 0.61$, respectively).

Discussion

By measuring DNA-binding kinetics of cTALE arrays that form 0.7, 1, and 1.4 superhelical turns, we probe the functional relevance of locally unfolded TALE states. We describe a novel method to glean mechanistic details from complex single molecule kinetics. In our simplified cTALE system, we find conformational heterogeneity in both DNA free and DNA-bound states. We find that association is slowed in arrays containing one full turn of repeats or more. Because most natural and designed TALEs contain more than a full turn of repeats, this finding has important implications for design of high affinity TALE endonucleases (TALEN) molecules, suggesting that placement of destabilized repeats at specific positions may increase activity.

340

341 **cTALEs containing NS RVD bind DNA with high affinity**

342 NS is an uncommon RVD in natural TALEs. Previous reports suggest that NS is
343 fairly nonspecific, but may bind with higher affinity than other common RVDs (NG, NI,
344 NN, and HD)(Miller et al., 2015). Our fitted rate constants can be used to calculate the
345 apparent K_d (K_{app}) calculated from using equation as follows:

346
$$K_{app} = \frac{[TALE-DNA + TALE^{*}-DNA]}{[DNA][TALE + TALE^{*}]} = \frac{K_{eq,DNA-free}K_2 + K_{eq,DNA-free}K_2K_{eq,DNA-bound}}{1+K_{eq,DNA-free}} = \frac{\frac{k_1}{k_{-1}} \times \frac{k_2}{k_{-2}}(1+\frac{k_3}{k_{-3}})}{1+\frac{k_1}{k_{-1}}} \quad (3)$$

347 where $K_2 = k_2/k_{-2}$.

348

349 Using fitted rate constants from Table 1 in the final equality in equation 3 gives values
350 for K_{app} of 2.5 nM for the 8 repeat cTALE array, 0.5 nM for the 12 repeat cTALE array,
351 and 1.0 nM for the 16 repeat cTALE array. Increasing the number of repeats has a
352 modest affect on the apparent K_d due to the increased population of binding
353 incompetent DNA free TALE in the 12, and 16 repeat arrays. This affinity change is
354 small compared to a previous report studying length dependence on affinity of designed
355 TALEs (dTALEs) showing the K_d of a dTALE decreased by a factor of two with the
356 addition of only 1.5 repeats (Rinaldi et al., 2017).

TALEs are believed to read out sequence information from one strand (Boch et al., 2009). Due to the asymmetry of our DNA sequences (poly-dA base-paired with poly-dT), in principle, the FRET efficiency contains information on the binding orientation (and thus strand preference). However, based on the crystal structure of the DNA-bound state of TAL-effector PthXo1 (Mak et al., 2012), we estimate that the distance between the donor site of $NcTALE_8$ (repeat 1) to the 5' acceptor site on the DNA (Cy5-A_{15}/T_{15}) should be similar for both the dA-sense or dT-sense orientations (Figure 4- figure supplement 3A). Thus, the FRET data does not discriminate between the two modes of binding for the eight-repeat construct. However, for the 16 repeat NS RVD cTALE arrays, the PthXo1 model suggests very different distances (25 Å versus 73 Å for the dT-sense or dA-sense respectively, Figure 4- figure supplement 3B) between the donor site (TALE repeat 14) and the acceptor site (5' Cy5-A_{23}/T_{23}). To restrict the number of binding positions available to longer cTALE arrays, the 23 base pair DNA used for $NcTALE_{16}$ measurements (as well as DNA depicted in Figure 4- figure supplement 3B) has the same number of additional base pairs as repeats (8 additional repeats and 8 additional base pairs) compared to the 15 base pair DNA used for $NcTALE_8$ measurements (as well as DNA depicted in Figure 4- figure supplement 3A). While we limited the number of available binding positions, it may be possible for cTALEs to slide along DNA. However, taking into account the four repeat N-terminal capping domain, there are only three available base pairs in the bound complex. Thus we don't expect the distance measurements to change by more than 10Å (~3 base pairs) if sliding occurs. The observation that there is colocalization but no measurable

379 FRET when $NcTALE_{16}$ is bound to DNA suggests that cTALEs containing the NS RVD
380 prefer adenine (the dA-sense mode) compared with thymine bases, consistent with
381 previous reports (Boch et al., 2009).
382
383 **Conformational heterogeneity in the unbound state may be caused by local**
384 **unfolding**
385 The cumulative distributions of dwell-times in Figure 3 provide clear evidence for
386 conformational heterogeneity in both the free and DNA-bound cTALEs. Although the
387 deterministic modeling supports such heterogeneity, puts it in the framework of a
388 molecular model, and provides a means to determine the microscopic rate and
389 equilibrium constants, such analysis provides little information about the structural
390 nature of TALE conformational heterogeneity.
391 Figure 6 shows a model of cTALE conformational change consistent with DNA
392 binding kinetics. In this model there are four TALE states. DNA-free cTALEs comprise
393 both incompetent and binding competent states. DNA-bound cTALES comprise
394 encounter and locked complexes with DNA. For 8 repeat cTALE arrays, the DNA-
395 binding competent state is more highly populated than the DNA-binding incompetent
396 state. In this reaction scheme, the DNA-binding incompetent state can be regarded as
397 an off-pathway conformation that inhibits DNA binding (Figure 6A).
398 Because the 8 repeat cTALE array does not form multiple turns of a superhelix,
399 unfolding to bind DNA is not required. In the model in Figure 6, the binding competent
400 state is the fully folded conformation, whereas the binding incompetent state includes

401 partly folded conformations. Consistent with this interpretation, increasing populations of
402 partly folded states through addition of 1M urea and through entropy enhancing
403 mutations decreases apparent binding rates of 8 repeat cTALEs (Figure 6- figure
404 supplement 1). This is also consistent with a partly folded DNA-binding incompetent
405 state in shorter cTALE arrays.

406 For 12 and 16 repeat cTALE arrays, the DNA-binding incompetent state is more
407 highly populated than the DNA-binding competent state. In the model in Figure 6, the
408 DNA-binding competent state is a high-energy conformation required for DNA binding
409 (Figure 6B-C). Because 12 and 16 repeat cTALEs are expected to form 1 and 1.4 turns
410 (excluding the N-terminal domain), we hypothesize that the binding competent state
411 includes some partly folded states that allow access to DNA. Not all partly folded states
412 open the array to access DNA; therefore, the binding incompetent state includes some
413 nonproductive partly folded states in addition to the fully folded state.

414 In arrays containing 12 or more cTALEs, the binding competent and binding
415 incompetent states likely include mixtures of many specific partly folded states. Because
416 the types of partly folded states are unknown, connecting equilibria between binding
417 competent and binding incompetent states to calculated partly folded equilibria (using
418 folding free energies similar to Figure 1) is challenging. Future work towards
419 understanding the structural characteristics of the binding competent state in TALE
420 arrays of one or more turns would inform which partly folded states to include in the
421 calculation, making this comparison meaningful. A better structural understanding of the
422 DNA binding competent state will also allow an opportunity for precise placement of

423 destabilized repeats in designed TALEN arrays which may enable more precise gene
424 editing methodologies in both clinical and basic research applications.
425
426 **TALE functional instability presents a new mode of transcription factor binding**
427 Here we demonstrate kinetic heterogeneity in DNA-bound and unbound TALE
428 arrays, and we subsequently link the observed heterogeneity to partial unfolding of
429 TALE arrays. We propose a model where binding requires partial unfolding of TALE
430 arrays longer than one superhelical turn providing a functional role for previously
431 observed moderate stability of TALE arrays. The functional instability described is
432 particularly surprising given the small population of partly folded states which we expect
433 to be DNA binding competent (partly folded states similar to internally unfolded and
434 interfacially fractured states depicted in Figure 1A). Discovery of a functional role for the
435 observed conformational heterogeneity is even more surprising, given the sequence
436 identity of each of our repeats. Sequence heterogeneity in naturally occurring TALE
437 arrays may further enable access to partly folded binding-competent states.
438 While it is well understood that many transcription factors sometimes undergo
439 local folding transition upon DNA binding (Spolar and Record, 1994; Tsafou et al.,
440 2018), the findings here indicate that for TALE arrays, the major conformer is fully
441 folded, and must undergo a local unfolding transition in order to bind DNA. Taken
442 together, these findings suggest a new mode of transcription factor binding and provide
443 compelling evidence for functional instability in TALE arrays.
444

Conformational heterogeneity in the bound state

Previous reports show that TALEs have multiple diffusional modes when searching nonspecific DNA (Cuculis et al., 2015). Our work suggests that cTALEs have multiple binding modes (encounter and locked states in Figure 6) indicating cTALEs undergo a conformational change also when bound to specific DNA sequences. Table 1 shows that microscopic rate constants for transition into and out of longer lived locked bound states become much slower in 12 and 16 repeat cTALEs compared with 8 repeat cTALEs (k_{-3} and k_3). These rate constants decrease much more than the microscopic unbinding rate constant (the k_{-2} values are 0.66 s^{-1}, 0.13 s^{-1}, and 0.299 s^{-1} for $NcTALE_8$, $NcTALE_{12}$, and $NcTALE_{16}$ respectively) suggesting a large conformational change that depends on the number of repeats. Although the model does not provide information on structure of this conformational change, it is possible this conformational change involves a slinky motion to decrease helical rise. Consistent with this hypothesis, crystal structures of TALEs in the free and DNA-bound state show 11.5 repeats per turn in both states, but the helical rise decreases upon binding (Deng et al., 2012). Another possibility involves specific interaction with RVDs and bases in the major groove of DNA. Crystal structures show little deformation of DNA structure, so bending of DNA seems unlikely. While we can only hypothesize about the structural nature of the conformational changes, deterministic simulations show that cTALEs bind DNA through short encounters which occasionally become long-lived locked conformations (Figure 6). Taken together, these findings indicate that functional instability plays a crucial role

in cTALE DNA binding, and demonstrate the importance of conformational dynamics in complex assembly.

Materials and Methods

Cloning, expression, purification, and labeling

Consensus TALE repeat constructs were cloned with C-terminal His_6 tags via an in-house version of Golden Gate cloning (Cermak et al., 2011). TALE constructs were grown in BL21(T1R) cells at 37°C to an OD of 0.6-0.8 and induced with 1 mM IPTG. Following cell pelleting and lysis, proteins were purified by resuspending the insoluble material in 6M urea, 300 mM NaCl, 0.5 mM TCEP, and 10 mM $NaPO_4$ pH 7.4. Constructs were loaded onto a Ni-NTA column. Protein was eluted using 250 mM imidazole and refolded during buffer exchange into 300 mM NaCl, 30% glycerol, 0.5 mM TCEP, and 10 mM $NaPO_4$ pH 7.4.

Labelling of cTALE arrays followed a previously reported protocol (Rasnik et al., 2004). $NcTALE_8$ and $NcTALE_{12}$ were labeled at residue R30C in the first repeat, while $NcTALE_{16}$ was labeled at residue R30C in the fourteenth repeat. 1 mg protein was loaded onto 500 uL NiNTA spin column. The column as washed with 10 column volumes of 300 mM NaCl, 0.5 mM TCEP, and 10 mM $NaPO_4$ pH 7.4. Tenfold molar excess Cy3 maleimide dye was resuspended in 10 μL DMSO and added to column. The column was rocked at room temperature for 30 minutes, then at 4°C overnight. Cy3-labeled protein was eluted with 250 mM imidazole, 300 mM NaCl, 30% glycerol,

0.5 mM TCEP, and 10 mM $NaPO_4$ pH 7.4. Protein was stored in 300 mM NaCl, 30% glycerol, 0.5 mM TCEP, and 10 mM $NaPO_4$ pH 7.4 at -80°C.

Oligonucleotides

Sequences used for binding studies were 5'-Cy5-A_{15}-3' and 5' T_{15}-3' duplex (Cy5-A_{15}/T_{15}) for 8 repeat binding studies, and 5'-Cy5-A_{23}-3' and 5' T_{23}-3' duplex (Cy5-A_{23}/T_{23}) for 12 and 16 repeat binding studies. DNA was annealed at 5 μM concentration with 1.2-fold molar excess unlabeled strand in 10 mM Tris pH 7.0, 30 mM NaCl.

Single-molecule detection and data analysis

Biotinylated quarts slides and glass coverslips were prepared as previously described (Rasnik et al., 2004). Cy3-labeled cTALEs were immobilized on biotinylated slides taking advantage of neutravidin interaction with biotinylated α-penta•His antibody which binds the His_6 cTALE tag. Slides were pretreated with blocking buffer (5 μL yeast tRNA, 5 μL BSA, 40 μL T50) before addition of 250 pM labeled cTALE. Cy5-labeled duplex DNA was mixed with imaging buffer (20 mM Tris pH 8.0, 200 mM KCl, 0.5 mg mL^{-1} BSA, 1 mg mL^{-1} glucose oxidase, 0.004 mg mL^{-1} catalase, 0.8% dextrose and saturated Trolox ~1mg mL^{-1}) and molecules were imagined using total internal reflection fluorescence microscopy. The time resolution was 50 msec for $NcTALE_8$ and 100 msec for $NcTALE_{16}$ and $NcTALE_{12}$. Collection and analysis was performed as previously described (Roy et al., 2008).

FRET histograms

A minimum of 20 short movies were collected, and the first 5 frames (50 msec exposure time) were used to generate smFRET histograms. FRET was calculated as

509 $I_A/(I_A+I_D)$ where I_A and I_D are donor-leakage and background corrected fluorescence
510 emission of acceptor (Cy5) and donor (Cy3) fluorophores. In competition experiments,
511 unlabeled DNA with the same sequence as labeled DNA was mixed at indicated
512 concentrations with labeled DNA prior to imaging.

513 **Dwell time analysis**

514 Long movies were collected with 50 msec exposure time for $NcTALE_8$ and 100
515 msec exposure time for $NcTALE_{16}$ and $NcTALE_{16}$. At least 20 representative traces at
516 each DNA concentration were selected and dwell times were determined by fitting as
517 previously described using HaMMy (McKinney et al., 2006) for FRET in $NcTALE_8$. Dwell
518 times in $NcTALE_{12}$ and $NcTALE_{16}$ colocalization experiments are determined by using a
519 thresholding procedure for Cy5 excitation (Figure 4- figure supplement 1). The algorithm
520 used to identify low and high emission states here is slightly different than previously
521 described thresholding algorithms (Blanco and Walter, 2010). To reduce the number of
522 incorrectly identified transitions arising from increased background and noise at higher
523 Cy5-labeled DNA concentrations, a thresholding algorithm with two limits was
524 implemented (see Figure 4- figure supplement 1). All FRET and colocalization data are
525 well described by models with two distinct states (0.0 FRET and ~0.45 FRET as well as
526 low colocalization and high colocalization). Dwell times of the same state (low versus
527 high FRET or low versus high colocalization) for all traces at a given DNA concentration
528 are compiled, and cumulative distribution is generated with spacing equal to imaging
529 exposure time.

To determine apparent rate constants using model-independent analysis, cumulative distributions were fitted with single and double exponential decays (Figure 3 and 4). Observed rates from exponential decay fits were plotted as a function of DNA concentration. Apparent rate constants were calculated as slope of DNA concentration-dependent observed rates or average of DNA concentration-independent observed rates.

Deterministic modeling

Equations 1a-1c and 2a-2c were numerically integrated using the ODE15s and ODE45 solver in MATLAB. Microscopic rate constants were adjusted to minimize the sum of squared residuals between ODE-determined concentration of bound or free TALE and single molecule cumulative distributions using lsqnonlin in MATLAB. 68% confidence intervals were estimated by performing 2000 or 8000 bootstrap iterations in which residuals from the best fit of the model to the data were randomly re-sampled (with replacement) and re-fitted. All scripts and source data required to run this MATLAB program called **De**terminstic **M**odeling for **A**nalysis of complex **S**ingle molecule **K**inetics (DeMASK) are publicly available on GitHub at https://github.com/kgeigers/DeMASK.

Acknowledgements

The authors thank members of the Barrick and Ha lab for their input on this work. The authors acknowledge the support of the Center for Molecular Biophysics at Johns Hopkins and Dr. Katherine Tripp for instrumental and technical support. Support to

KGS was provided by NIH training grant T32-GM008403. Support for this project was provided by NIH grant 1R01-GM068462 to DB and GM112659 to TH.

554 **References**

555 Aksel, T., Majumdar, A., Barrick, D., 2011. The contribution of entropy, enthalpy, and
556 hydrophobic desolvation to cooperativity in repeat-protein folding. Struct. Lond.
557 Engl. 1993 19, 349–360. https://doi.org/10.1016/j.str.2010.12.018
558 Blanco, M., Walter, N., 2010. Analysis of Complex Single Molecule FRET Time
559 Trajectories. Methods Enzymol. 472, 153–178. https://doi.org/10.1016/S0076-
560 6879(10)72011-5
561 Boch, J., Bonas, U., 2010. Xanthomonas AvrBs3 family-type III effectors: discovery and
562 function. Annu. Rev. Phytopathol. 48, 419–436. https://doi.org/10.1146/annurev-
563 phyto-080508-081936
564 Boch, J., Scholze, H., Schornack, S., Landgraf, A., Hahn, S., Kay, S., Lahaye, T.,
565 Nickstadt, A., Bonas, U., 2009. Breaking the code of DNA binding specificity of
566 TAL-type III effectors. Science 326, 1509–1512.
567 https://doi.org/10.1126/science.1178811
568 Cermak, T., Doyle, E.L., Christian, M., Wang, L., Zhang, Y., Schmidt, C., Baller, J.A.,
569 Somia, N.V., Bogdanove, A.J., Voytas, D.F., 2011. Efficient design and assembly
570 of custom TALEN and other TAL effector-based constructs for DNA targeting.
571 Nucleic Acids Res. 39, e82. https://doi.org/10.1093/nar/gkr218
572 Christian, M., Cermak, T., Doyle, E.L., Schmidt, C., Zhang, F., Hummel, A., Bogdanove,
573 A.J., Voytas, D.F., 2010. Targeting DNA Double-Strand Breaks with TAL Effector
574 Nucleases. Genetics 186, 757–761. https://doi.org/10.1534/genetics.110.120717
575 Cong, L., Zhou, R., Kuo, Y.-C., Cunniff, M., Zhang, F., 2012. Comprehensive
576 interrogation of natural TALE DNA-binding modules and transcriptional repressor
577 domains. Nat. Commun. 3, 968. https://doi.org/10.1038/ncomms1962
578 Cuculis, L., Abil, Z., Zhao, H., Schroeder, C.M., 2015. Direct observation of TALE
579 protein dynamics reveals a two-state search mechanism. Nat. Commun. 6, 7277.
580 https://doi.org/10.1038/ncomms8277
581 Deng, D., Yan, C., Pan, X., Mahfouz, M., Wang, J., Zhu, J.-K., Shi, Y., Yan, N., 2012.
582 Structural basis for sequence-specific recognition of DNA by TAL effectors.
583 Science 335, 720–723. https://doi.org/10.1126/science.1215670
584 edited by S. E. Harding, A.J.R., 1992. Analytical ultracentrifugation in biochemistry and
585 polymer science. Royal Society of Chemistry, Cambridge [England].
586 Gao, H., Wu, X., Chai, J., Han, Z., 2012. Crystal structure of a TALE protein reveals an
587 extended N-terminal DNA binding region. Cell Res. 22, 1716–1720.
588 https://doi.org/10.1038/cr.2012.156
589 Geiger-Schuller, K., Barrick, D., 2016. Broken TALEs: Transcription Activator-like
590 Effectors Populate Partly Folded States. Biophys. J. 111, 2395–2403.
591 https://doi.org/10.1016/j.bpj.2016.10.013
592 Geiger-Schuller, K., Sforza, K., Yuhas, M., Parmeggiani, F., Baker, D., Barrick, D.,
593 2018. Extreme stability in de novo-designed repeat arrays is determined by
594 unusually stable short-range interactions. Proc. Natl. Acad. Sci. 201800283.
595 https://doi.org/10.1073/pnas.1800283115

596 Geissler, R., Scholze, H., Hahn, S., Streubel, J., Bonas, U., Behrens, S.-E., Boch, J.,
597 2011. Transcriptional activators of human genes with programmable DNA-
598 specificity. PloS One 6, e19509. https://doi.org/10.1371/journal.pone.0019509
599 Kay, S., Hahn, S., Marois, E., Hause, G., Bonas, U., 2007. A bacterial effector acts as a
600 plant transcription factor and induces a cell size regulator. Science 318, 648–
601 651. https://doi.org/10.1126/science.1144956
602 Li, T., Huang, S., Jiang, W.Z., Wright, D., Spalding, M.H., Weeks, D.P., Yang, B., 2011.
603 TAL nucleases (TALNs): hybrid proteins composed of TAL effectors and FokI
604 DNA-cleavage domain. Nucleic Acids Res. 39, 359–372.
605 https://doi.org/10.1093/nar/gkq704
606 Li, Y., Moore, R., Guinn, M., Bleris, L., 2012. Transcription activator-like effector hybrids
607 for conditional control and rewiring of chromosomal transgene expression. Sci.
608 Rep. 2, 897. https://doi.org/10.1038/srep00897
609 Ma, H., Reyes-Gutierrez, P., Pederson, T., 2013. Visualization of repetitive DNA
610 sequences in human chromosomes with transcription activator-like effectors.
611 Proc. Natl. Acad. Sci. U. S. A. 110, 21048–21053.
612 https://doi.org/10.1073/pnas.1319097110
613 Maeder, M.L., Angstman, J.F., Richardson, M.E., Linder, S.J., Cascio, V.M., Tsai, S.Q.,
614 Ho, Q.H., Sander, J.D., Reyon, D., Bernstein, B.E., Costello, J.F., Wilkinson,
615 M.F., Joung, J.K., 2013. Targeted DNA demethylation and activation of
616 endogenous genes using programmable TALE-TET1 fusion proteins. Nat.
617 Biotechnol. 31, 1137–1142. https://doi.org/10.1038/nbt.2726
618 Mahfouz, M.M., Li, L., Piatek, M., Fang, X., Mansour, H., Bangarusamy, D.K., Zhu, J.-
619 K., 2012. Targeted transcriptional repression using a chimeric TALE-SRDX
620 repressor protein. Plant Mol. Biol. 78, 311–321. https://doi.org/10.1007/s11103-
621 011-9866-x
622 Mak, A.N.-S., Bradley, P., Cernadas, R.A., Bogdanove, A.J., Stoddard, B.L., 2012. The
623 crystal structure of TAL effector PthXo1 bound to its DNA target. Science 335,
624 716–719. https://doi.org/10.1126/science.1216211
625 McKinney, S.A., Joo, C., Ha, T., 2006. Analysis of single-molecule FRET trajectories
626 using hidden Markov modeling. Biophys. J. 91, 1941–1951.
627 https://doi.org/10.1529/biophysj.106.082487
628 Miller, J.C., Zhang, L., Xia, D.F., Campo, J.J., Ankoudinova, I.V., Guschin, D.Y.,
629 Babiarz, J.E., Meng, X., Hinkley, S.J., Lam, S.C., Paschon, D.E., Vincent, A.I.,
630 Dulay, G.P., Barlow, K.A., Shivak, D.A., Leung, E., Kim, J.D., Amora, R., Urnov,
631 F.D., Gregory, P.D., Rebar, E.J., 2015. Improved specificity of TALE-based
632 genome editing using an expanded RVD repertoire. Nat. Methods 12, 465–471.
633 https://doi.org/10.1038/nmeth.3330
634 Miyanari, Y., Ziegler-Birling, C., Torres-Padilla, M.-E., 2013. Live visualization of
635 chromatin dynamics with fluorescent TALEs. Nat. Struct. Mol. Biol. 20, 1321–
636 1324. https://doi.org/10.1038/nsmb.2680
637 Moscou, M.J., Bogdanove, A.J., 2009. A simple cipher governs DNA recognition by TAL
638 effectors. Science 326, 1501. https://doi.org/10.1126/science.1178817

639 Newville, M., Stensitzki, T., Allen, D.B., Ingargiola, A., 2014. LMFIT: Non-Linear Least-
640 Square Minimization and Curve-Fitting for Python¶. Zenodo.
641 https://doi.org/10.5281/zenodo.11813
642 O'Donnell, M., Kuriyan, J., 2006. Clamp loaders and replication initiation. Curr. Opin.
643 Struct. Biol. 16, 35–41. https://doi.org/10.1016/j.sbi.2005.12.004
644 Rasnik, I., Myong, S., Cheng, W., Lohman, T.M., Ha, T., 2004. DNA-binding Orientation
645 and Domain Conformation of the E.coli Rep Helicase Monomer Bound to a
646 Partial Duplex Junction: Single-molecule Studies of Fluorescently Labeled
647 Enzymes. J. Mol. Biol. 336, 395–408. https://doi.org/10.1016/j.jmb.2003.12.031
648 Rinaldi, F.C., Doyle, L.A., Stoddard, B.L., Bogdanove, A.J., 2017. The effect of
649 increasing numbers of repeats on TAL effector DNA binding specificity. Nucleic
650 Acids Res. https://doi.org/10.1093/nar/gkx342
651 Römer, P., Hahn, S., Jordan, T., Strauss, T., Bonas, U., Lahaye, T., 2007. Plant
652 pathogen recognition mediated by promoter activation of the pepper Bs3
653 resistance gene. Science 318, 645–648. https://doi.org/10.1126/science.1144958
654 Roy, R., Hohng, S., Ha, T., 2008. A practical guide to single-molecule FRET. Nat.
655 Methods 5, 507–516. https://doi.org/10.1038/nmeth.1208
656 Spolar, R.S., Record, M.T., 1994. Coupling of local folding to site-specific binding of
657 proteins to DNA. Science 263, 777–784.
658 Tsafou, K., Tiwari, P.B., Forman-Kay, J.D., Metallo, S.J., Toretsky, J.A., 2018. Targeting
659 Intrinsically Disordered Transcription Factors: Changing the Paradigm. J. Mol.
660 Biol., Intrinsically Disordered Proteins 430, 2321–2341.
661 https://doi.org/10.1016/j.jmb.2018.04.008
662 Zhang, F., Cong, L., Lodato, S., Kosuri, S., Church, G.M., Arlotta, P., 2011. Efficient
663 construction of sequence-specific TAL effectors for modulating mammalian
664 transcription. Nat. Biotechnol. 29, 149–153. https://doi.org/10.1038/nbt.1775
665

666

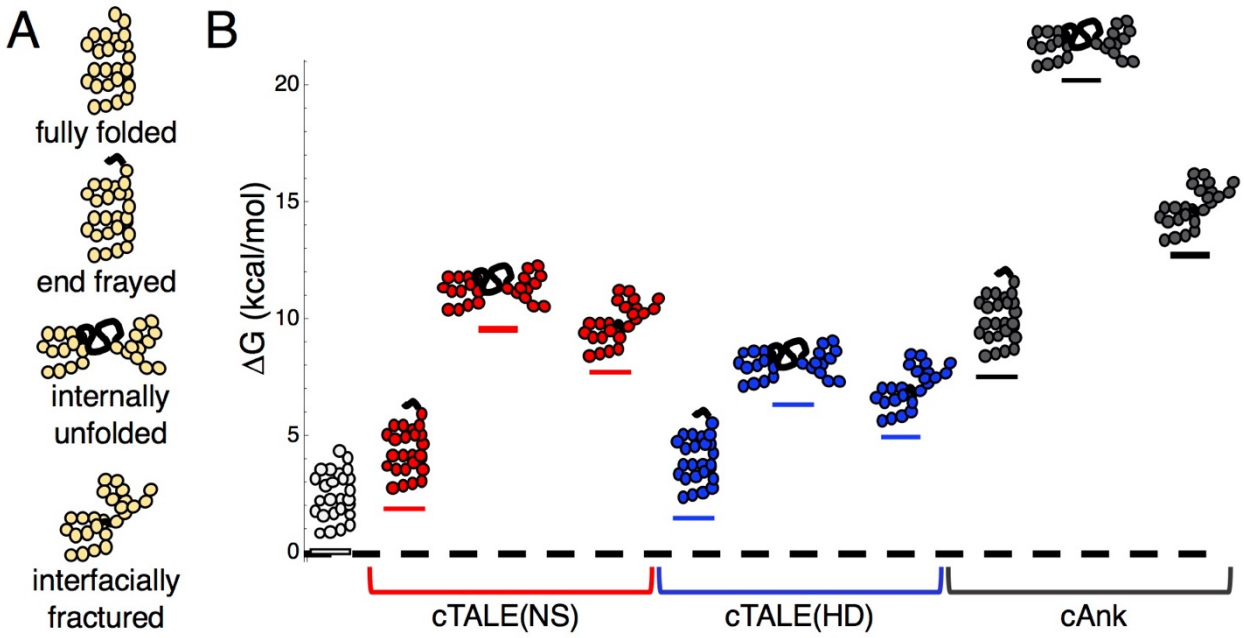

667

668 **Figure 1. cTALEs populate partly folded states.** (A) Cartoon of different partly folded
669 TALE conformational states. End-frayed states have one (or more) terminal repeats
670 unfolded. Internally unfolded states have a central repeat unfolded. Interfacially
671 fractured states have a disrupted interface between adjacent repeats. (B) Free energies
672 of partly folded states, calculated from previously published measurements and analysis
673 (Geiger-Schuller and Barrick, 2016), relative to the fully folded state, for consensus
674 TALE repeats with the NS repeat-variable diresidue sequence (cTALE(NS), red),
675 consensus TALE repeats with the HD repeat-variable diresidue sequence (cTALE(HD),
676 blue), and consensus ankyrin repeats (cAnk, black).

677

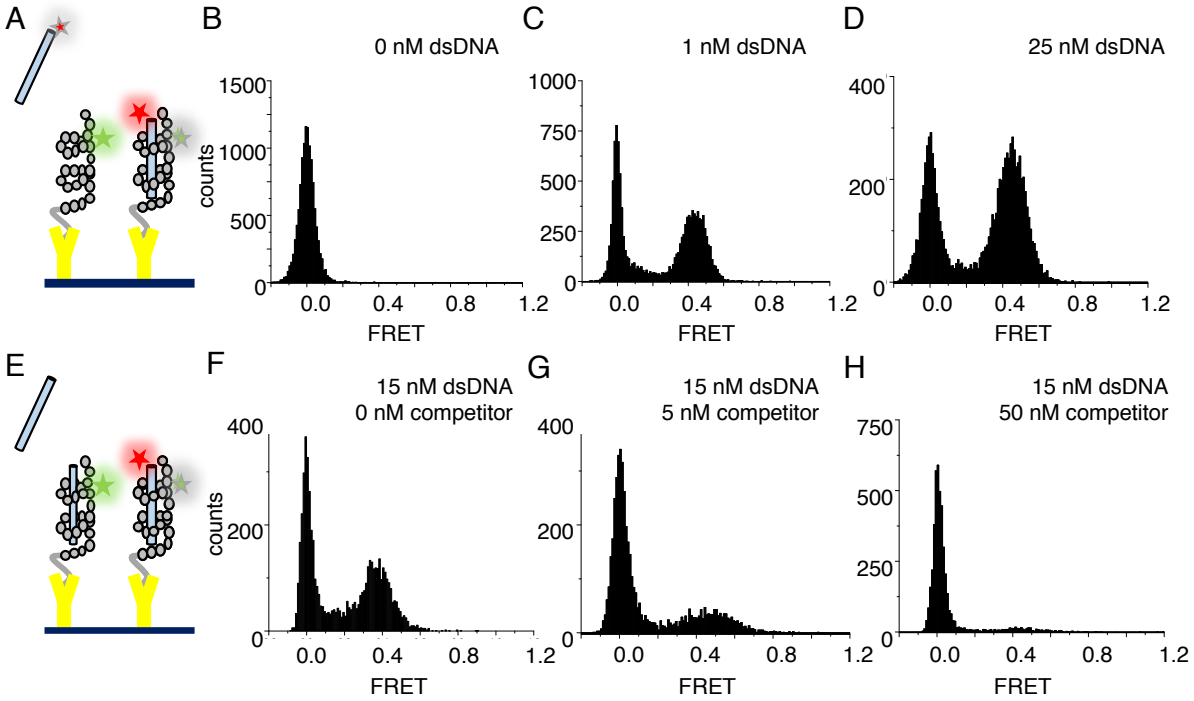

678

679 **Figure 2. cTALEs bind dsDNA reversibly.** (A) Schematic of single-molecule FRET
680 assay, with donor-labelled cTALE attached to a surface, and acceptor-labelled DNA free
681 in solution. (B-D) Single molecule FRET histograms show the appearance of a peak at
682 a FRET efficiency of 0.45 with increasing labelled DNA, consistent with a DNA-bound
683 cTALE. (E) Schematic of single-molecule FRET competition assay, with donor-labelled
684 cTALE attached to a surface, and acceptor-labelled DNA as well as competitor
685 unlabeled DNA free in solution. (F-H) Single molecule FRET histograms show the
686 disappearance of the peak at 0.45 FRET efficiency with increasing unlabeled competitor
687 DNA. Conditions: 20 mM Tris pH 8.0, 200 mM KCl.

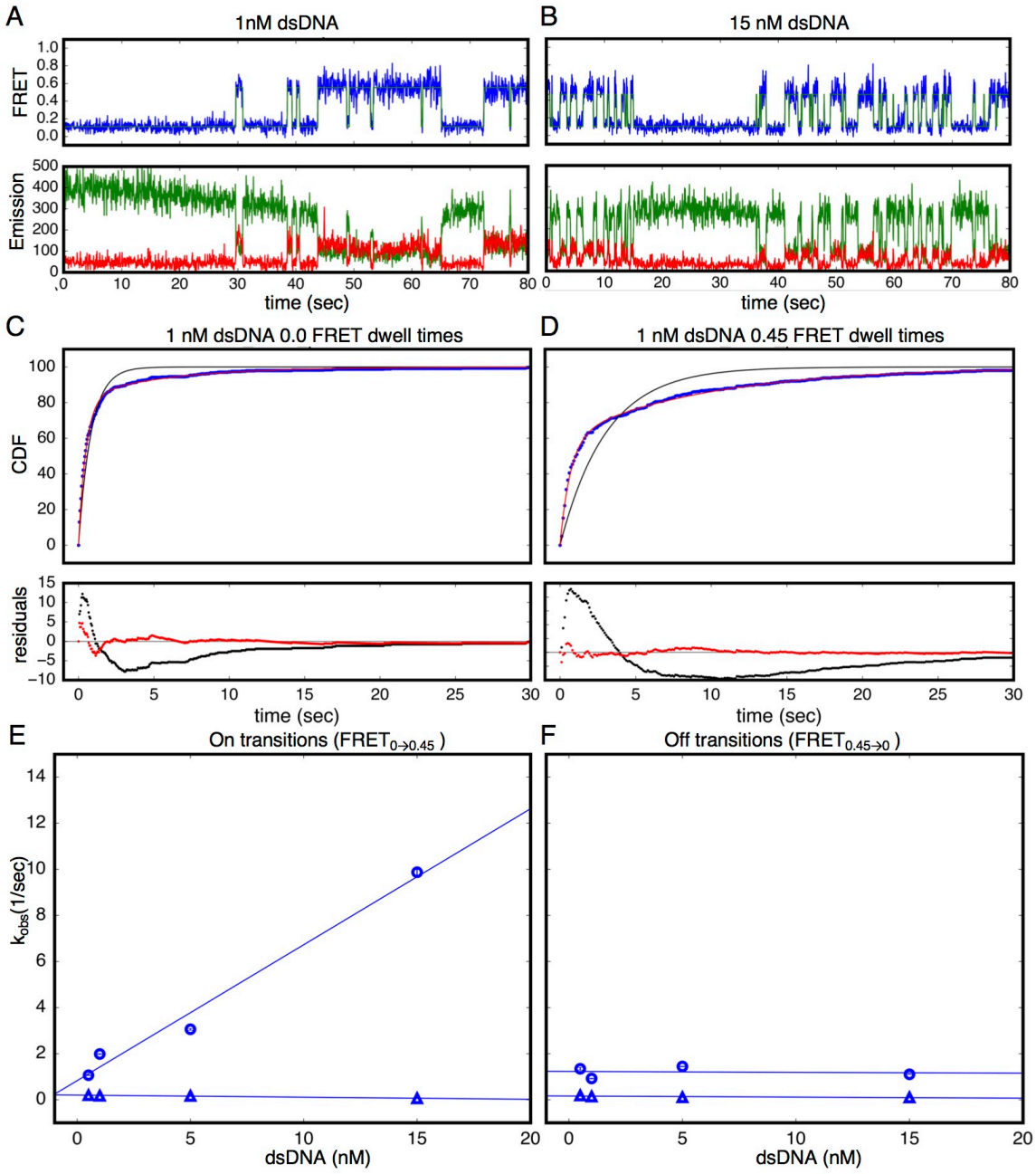

688

689 **Figure 3. Single Molecule (SM) kinetics show multiple phases in binding and**

690 **unbinding kinetics.** (A-B) Long time trajectories showing transitions between low- and

691 high-FRET states (efficiencies of 0 and 0.45). The top panel shows calculated FRET

692 efficiency in blue and two-state Hidden Markov Model fit in green (McKinney et al.,

693 2006). The bottom panels show Cy3 and Cy5 fluorescence emission in green and red

694 respectively. At low DNA concentration (A), the low FRET state predominates. As DNA
695 concentration is increased (B), more time is spent in the high FRET state, because the
696 dwell times in the low FRET state are shorter. At low DNA concentrations, there
697 appears to be long- and short-lived high-FRET states. Likewise, at near-saturating DNA
698 concentrations, there appear to be long and short-lived low FRET states. (C, D)
699 Cumulative distributions of low- and high-FRET dwell times (blue circles). Fits to single-
700 exponentials (black) show large nonrandom residuals (lower panels), consistent with the
701 heterogeneity noted in (A) and (B). Double-exponentials (red) give smaller, more
702 uniform residuals. (E) Apparent association rate constants as a function of DNA
703 concentration. The apparent rate constants for the fast phase depend on DNA
704 concentration (blue circles), indicating a bimolecular step binding event. The apparent
705 rate constants for the slow phase do not depend on DNA-concentration (blue triangles),
706 suggesting an isomerization event. (F) Apparent dissociation rate constants as a
707 function of DNA concentration (phase 1 shown in blue circles, and phase 2 shown in
708 blue triangles). Neither phase shows a DNA concentration dependence, indicating a
709 dissociation and/or isomerization events. 67.4% confidence intervals are estimated
710 using the conf_interval function of lmfit by performing F-tests (Newville et al., 2014).
711 Conditions: 20 mM Tris pH 8.0, 200 mM KCl.
712 **Figure supplement 1**. Alternating laser experiments show agreement between $cTALE_8$
713 FRET and colocalization kinetics.
714 **Figure supplement 2**. cTALEs do not slide onto ends of short dsDNA.
715 **Source data 1.** List of values used to construct long time trajectories.

716 **Source data 2.** List of values used to construct CDFs.

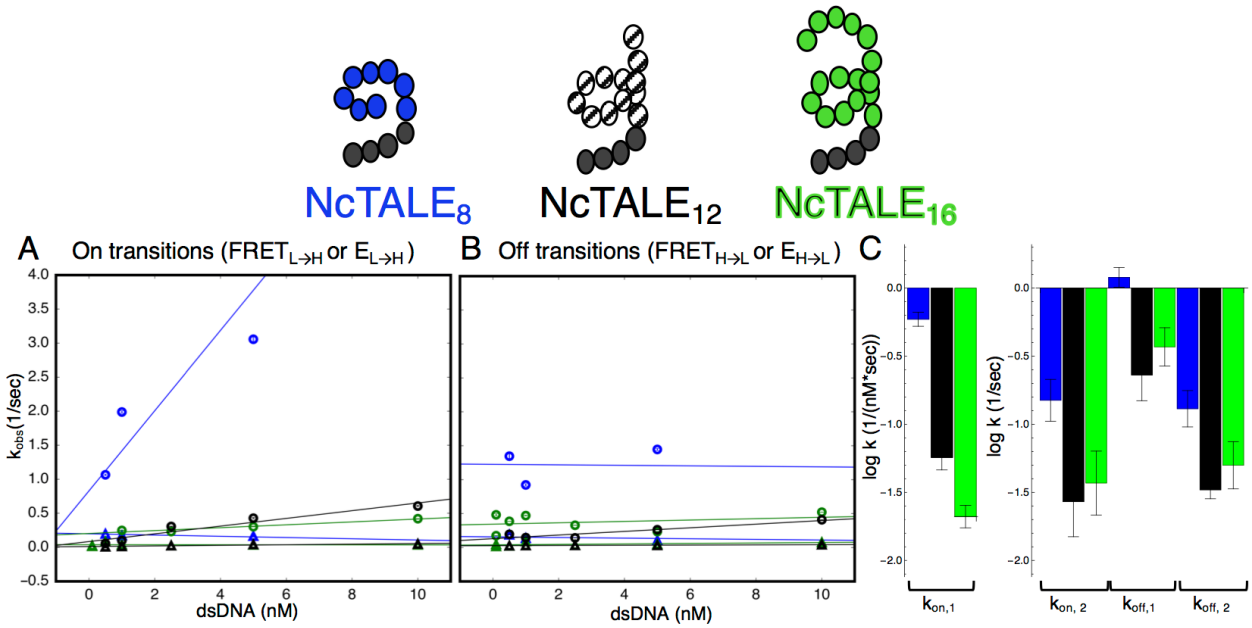

Figure 4. A 16-repeat TALE protein binds and unbinds DNA more slowly than an eight repeat protein. (A) Apparent association rate constants as a function of DNA concentration for an 8 repeat cTALE (blue), a 12 repeat cTALE (black), and a 16 repeat cTALE (green). 8 repeat TALE kinetics are measured by FRET ($FRET_{L\rightarrow H}$) while 12 and 16 repeat TALE kinetics are measured by colocalization ($E_{L\rightarrow H}$). The apparent rate constants for the fast phase of binding are DNA concentration dependent (blue, black, and green circles), indicating a bimolecular binding event. The DNA concentration-dependence is greatest (larger slope) for the 8 repeat cTALE. The apparent rate constants for the slow phase do not depend on DNA-concentration (blue, black, and green triangles), suggesting an isomerization event. (B) Apparent dissociation rate constants as a function of DNA concentration (phase 1 shown in circles, and phase 2 shown in triangles). Neither phase shows a DNA concentration dependence, indicating a dissociation and/or isomerization events. Rate constants for all phases are slower for

the 12-repeat construct (black) and 16-repeat construct (green) than for the 8-repeat construct (blue), particularly for the bimolecular binding step. (C) Log_{10} of rate constants for 8 (blue), 12 (black), and 16(green) repeat cTALEs. Units of the bimolecular binding rate constant are $nM^{-1}s^{-1}$, other unimolecular rate constants have units s^{-1}. 67.4% confidence intervals are estimated using the conf_interval function of lmfit by performing F-tests (Newville et al., 2014). Conditions: 20 mM Tris pH 8.0, 200 mM KCl.

Figure supplement 1. Colocalization trajectories show TALE-DNA binding and unbinding events.

Figure supplement 2. Bound and unbound lifetimes of 16- and 12-repeat TALE proteins are consistent with multiphasic binding and unbinding.

Figure supplement 3. Distance estimates between labeling sites for $NcTALE_8$ and $NcTALE_{16}$ and the 5' ends of bound DNA.

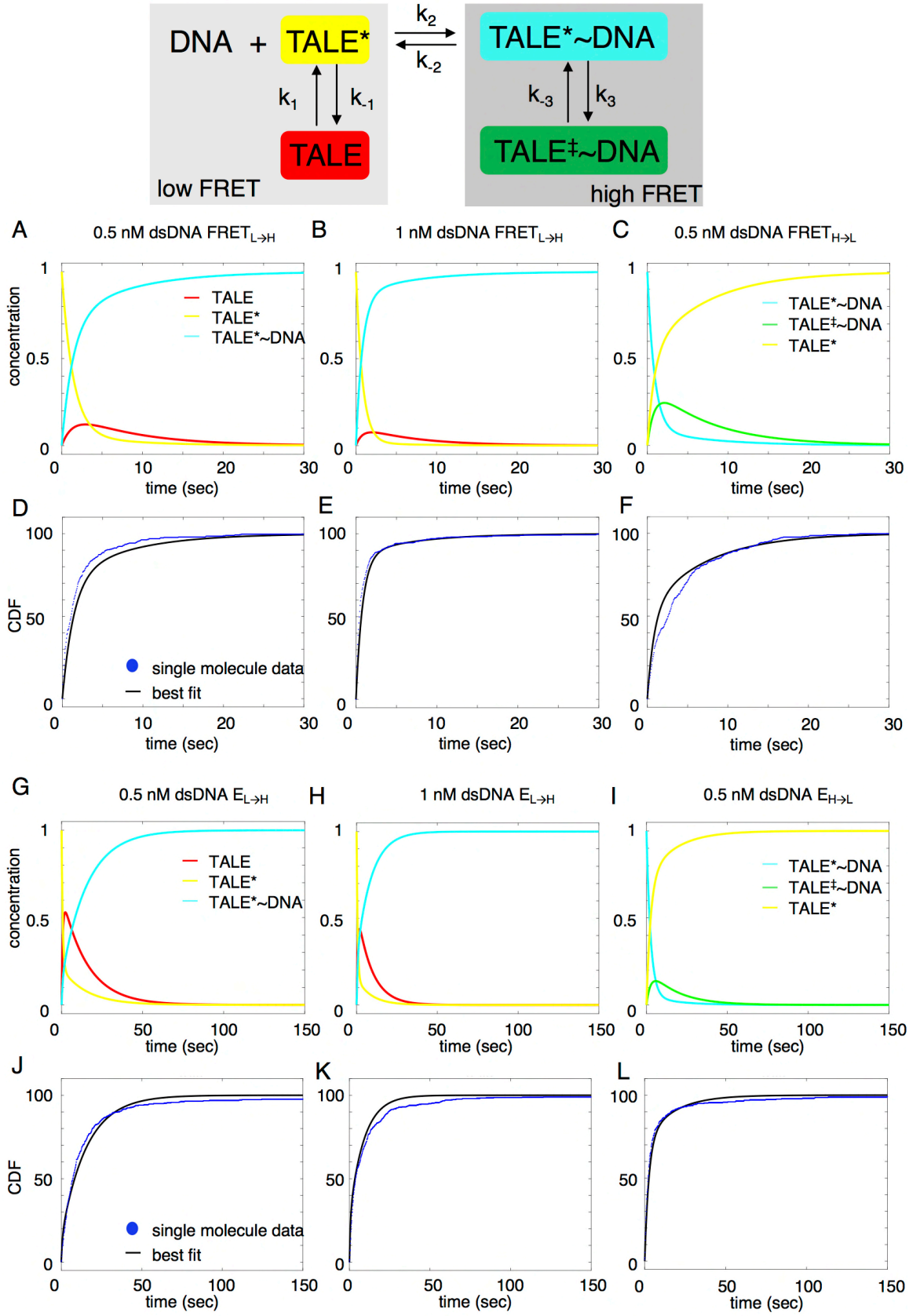

745

746 **Figure 5. Deterministic simulations provide evidence for conformational**
747 **heterogeneity in the unbound state.** The model most consistent with data is shown at
748 the top. Unbound TALEs can exist in DNA-binding competent (TALE*) or DNA-binding
749 incompetent (TALE) states. DNA-bound TALEs can exist in short-lived (TALE*~DNA) or
750 long-lived ($TALE^{\ddagger}$~DNA) DNA-bound states. Cumulative distributions of dwell-times
751 (shown as blue points) from 8 repeat single-molecule time trajectories (A-F) and 16
752 repeat single-molecule time trajectories (G-L) were analyzed with the model (best-fit
753 shown in black). (A-C and G-I) Populations of states as a function of time, generated by
754 numerical integration in Matlab. (D-F and J-L) Cumulative distributions in blue circles
755 and best fit lines are shown in black. Best-fit microscopic rate constants and 68%
756 confidence intervals are listed in Table 1.
757

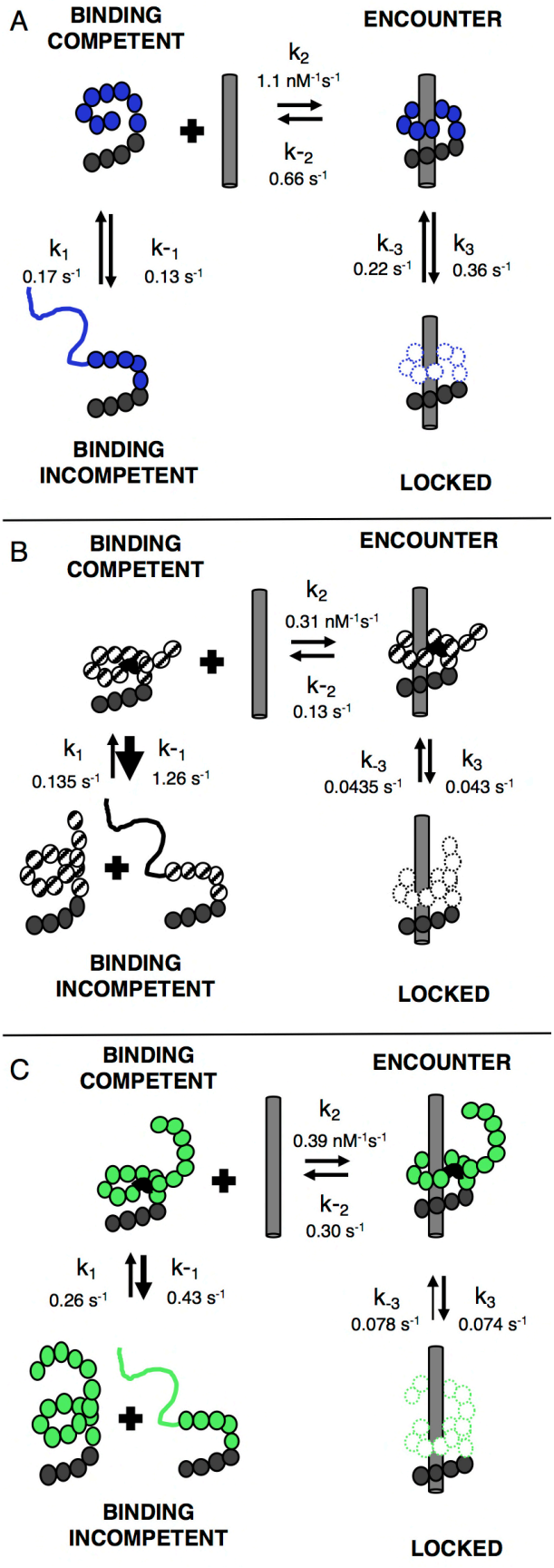

758

759 **Figure 6. TALEs with multiple superhelical turns must break to bind DNA.** Single-
760 molecule FRET studies and deterministic modeling support a model where TALEs exist
761 in four states: binding incompetent, binding competent, encounter complex, and locked.
762 In this model, for TALEs that form less than one full superhelical turn (8 repeats, A),
763 partly folded states are off-pathway and slow down binding. For longer TALEs that form
764 one (12, B) or more (16, C) complete superhelical turns, partial unfolding is required for
765 binding. DNA-bound TALEs form both encounter complexes and higher-affinity locked
766 conformations. Dynamics of long (12 and 16-repeat; B-C) TALEs bound to DNA are
767 significantly slower than for the shorter (8-repeat; A) TALE.
768 **Figure supplement 1**. Urea and destabilizing mutations decrease apparent binding rate
769 of cTALE$_8$.
770

Table 1. Kinetic parameters obtained from deterministic simulation fits.

	k_1 (sec^{-1})	k_{-1} (sec^{-1})	$K_{eq,\ DNA\text{-}free}$	k_2($sec^{-1}nM^{-1}$)	k_{-2} (sec^{-1})	k_3 (sec^{-1})	k_{-3} (sec^{-1})	$K_{eq,\ DNA\text{-}bound}$ (nM^{-1})
NcTALE$_8$ [a]	0.17 [0.16, 0.18]	0.13 [0.12, 0.14]	1.32 [1.26, 1.39]	1.1 [1.08, 1.12]	0.66 [0.65, 0.67]	0.36 [0.35, 0.37]	0.222 [0.218, 0.227]	1.62 [1.58, 1.66]
NcTALE$_{12}$ [b]	0.135 [0.133, 0.137]	1.26 [1.09, 1.34]	0.11 [0.10, 0.12]	0.31 [0.28, 0.33]	0.130 [0.129, 0.131]	0.043 [0.042, 0.044]	0.0435 [0.0428, 0.0442]	0.99 [0.97, 1.00]
NcTALE$_{16}$ [a]	0.26 [0.25, 0.27]	0.43 [0.39, 0.47]	0.61 [0.57, 0.64]	0.39 [0.38, 0.41]	0.299 [0.298, 0.300]	0.074 [0.073, 0.076]	0.078 [0.076, 0.079]	0.96 [0.95, 0.97]

68% confidence intervals shown in brackets are from 2,000[a] and 8,000[b] iterations of bootstrap analysis.

771

Supplemental Material

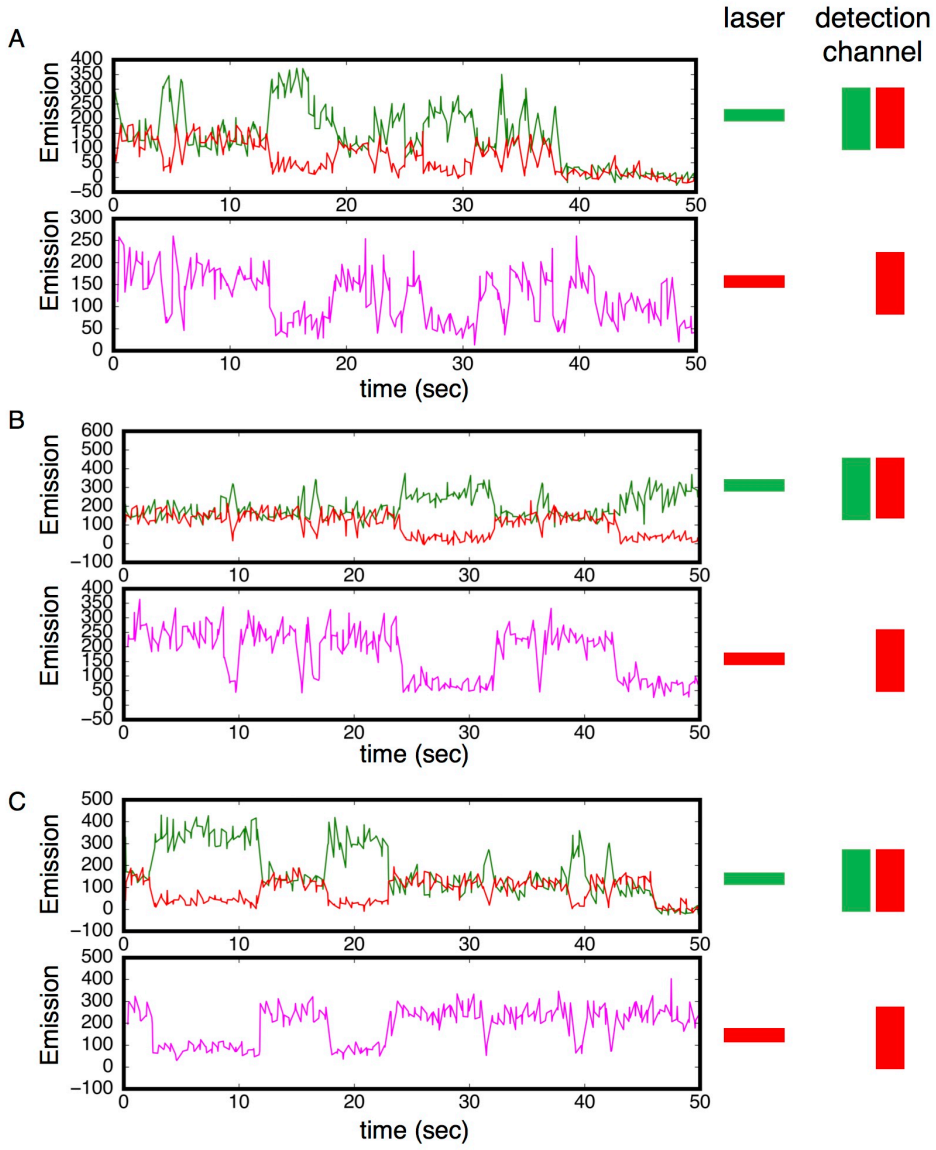

Figure 3- figure supplement 1. Alternating laser experiments show agreement between cTALE$_8$ FRET and colocalization kinetics. (A-C) Three representative time trajectories. In these trajectories, excitation alternated between red and green with 250 msec at each color. Top panels show detection of red and green light resulting from green laser excitation. High red (and low green) fluorescence result from FRET. Lower panels show detection of red light resulting from red laser excitation. There is strong

780 correlation between periods of high FRET in the upper panels (high red fluorescence,

781 low green fluorescence) and periods of high red fluorescence (from DNA binding) in the

782 lower panel. Conditions: 200 mM KCl, 20 mM Tris pH 8.0.

783

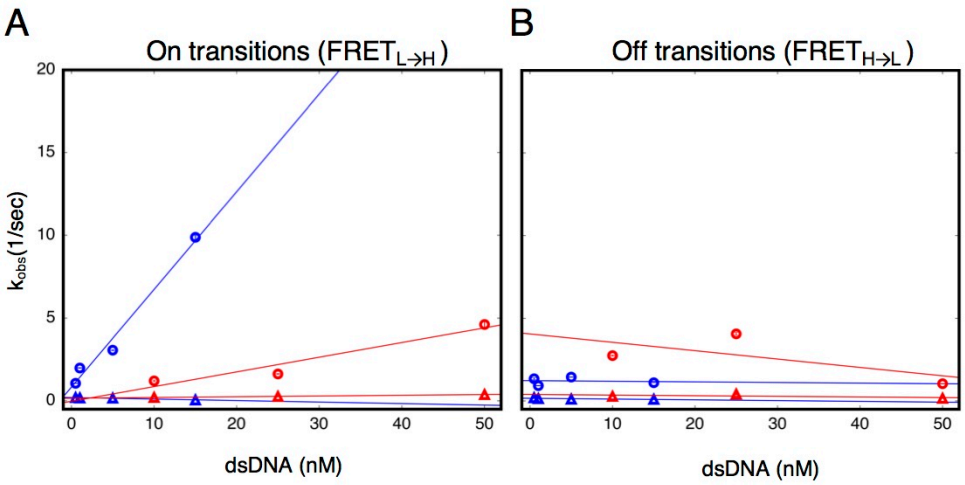

784

785 **Figure 3 – figure supplement 2. cTALEs do not slide onto ends of short dsDNA.**

786 Apparent association and dissociation rate constants as a function of DNA

787 concentration for an 8 repeat cTALE array (NcTALE$_8$) binding to uncapped (blue) and

788 capped (red) DNA, measured by single molecule FRET dwell time analysis. (A) Rate

789 constants for conversion from the low to the high FRET state (FRET$_{L\rightarrow H}$). Rate

790 constants for the faster phase increase with DNA concentration (circles), indicating a

791 bimolecular event. The DNA concentration-dependence is stronger (larger slope, k=0.59

792 ± 0.08 nM^{-1} sec^{-1}) with uncapped DNA than with capped DNA (k=0.09 ± 0.05 nM^{-1} sec^{-}

793 ^{1}), which is likely a result of the faster diffusion of small, uncapped DNA (10 kDa)

794 compared to large, capped DNA (320 kDa). Rate constants for the slower phase are not

795 DNA-concentration dependent (triangles). (B) Rate constants for conversion from the

796 high to the low FRET state (FRET$_{H\rightarrow L}$). Neither phase shows a DNA concentration

797 dependent, indicating unimolecular steps. Conditions: 200 mM KCl, 20 mM Tris pH 8.0.

798

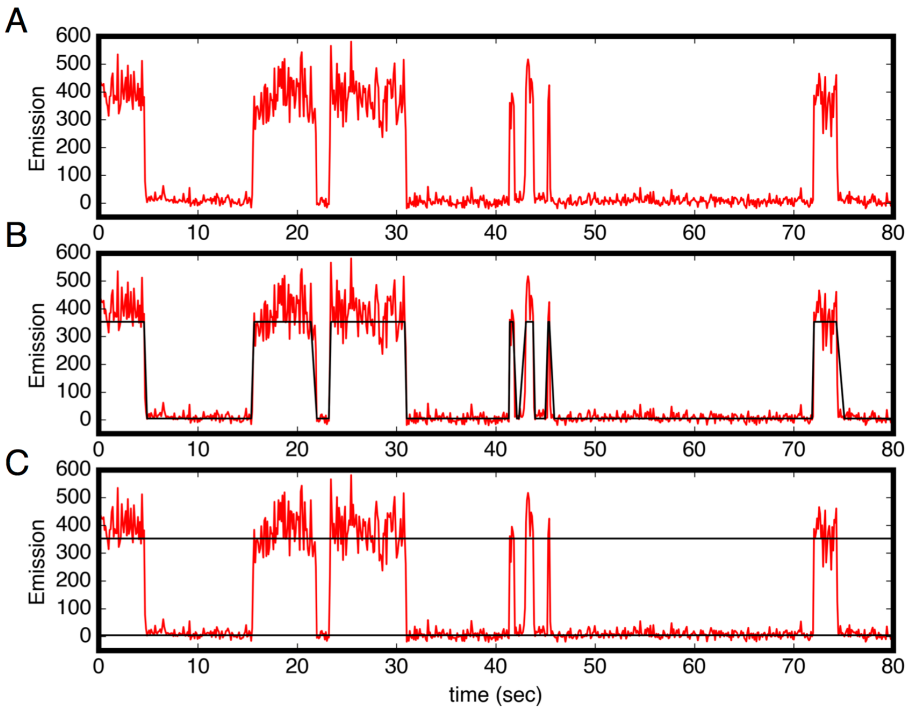

Figure 4- figure supplement 1. Colocalization trajectories show TALE-DNA binding and unbinding events. (A-C) One representative time trajectory and colocalization analysis for a sixteen repeat TALE, $NcTALE_{16}$, incubated with 1 nM Cy5-A_{15}/T_{15}. In the colocalization protocol, both the green and red lasers were used in the first ten frames (not shown) to identify single molecule locations. For all subsequent frames, Cy5-labeled DNA was continuously excited with the red laser. Red light emission images (from Cy5) were collected with time steps of 100 msec. Trajectories were generated from sites of red/green colocalization in the first ten frames, and were corrected for background Cy5 emission (red trajectories above). For each trajectory, we set two thresholds for low and high Cy5 emission (C). A molecule is designated to be in the high emission (DNA-bound) state above the high threshold, and in the low emission state below the low threshold. From this state-assignment procedure, dwell-times were

812 determined in the high (bound) and low (unbound) states (C). Conditions: 200 mM KCl,

813 20 mM Tris pH 8.0.

814

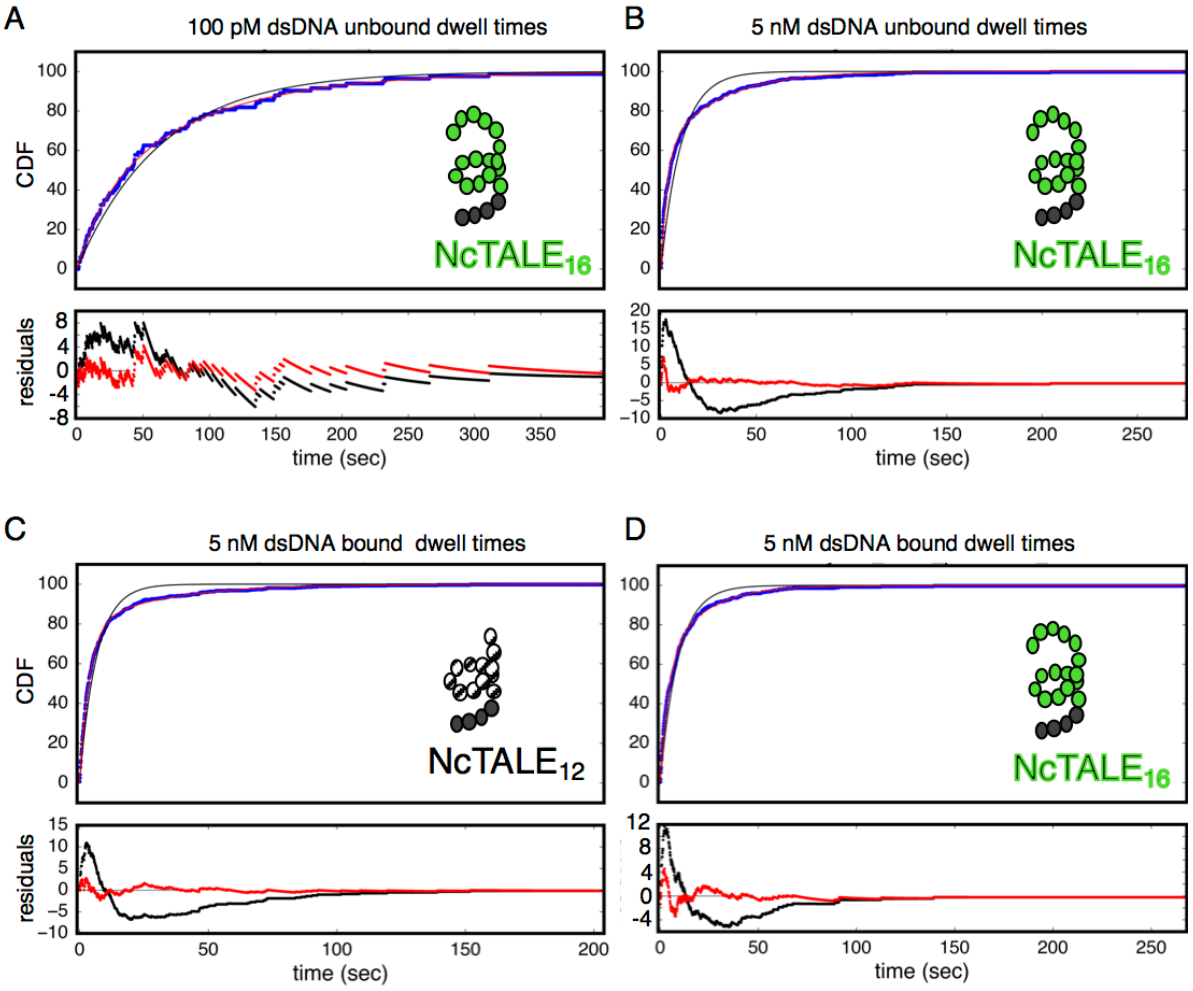

Figure 4- figure supplement 2. Bound and unbound lifetimes of 16- and 12-repeat TALE proteins are consistent with multiphasic binding and unbinding. (A, B) Cumulative distributions of low-FRET dwell times (blue circles) for a 16-repeat construct at low and high DNA concentration. Fits to single-exponentials (black) show large nonrandom residuals (lower panels) which are most pronounced at high DNA concentrations, consistent with the binding heterogeneity observed in eight repeat cTALEs (Figure 3). Double-exponentials (red) give smaller, more uniform residuals. (C, D) Cumulative distributions of high-FRET dwell times (blue circles) for 16- and 12-

repeat constructs at high DNA concentration. Fits to single-exponentials (black) show large nonrandom residuals (lower panels), consistent with the dissociation heterogeneity observed in eight repeat cTALEs. Double-exponentials (red) give smaller, more uniform residuals.

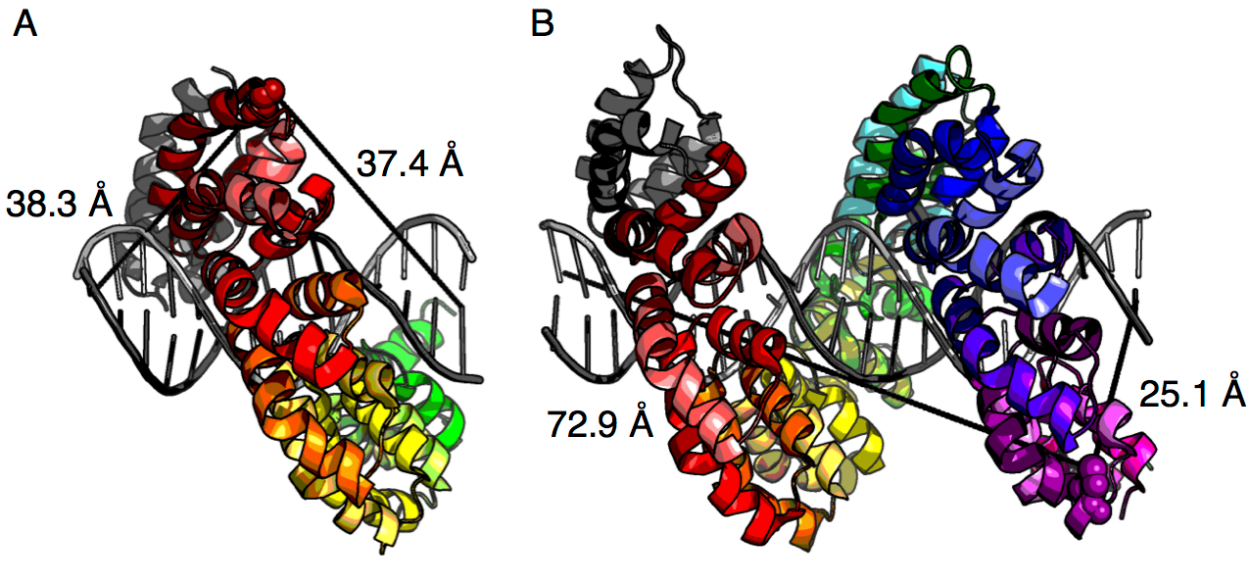

Figure 4- figure supplement 3. Distance estimates between labeling sites for NcTALE$_8$ and NcTALE$_{16}$ and the 5' ends of bound DNA. The crystal structure of PthXo1 (PDB: 3UGM) (Mak et al., 2012) in complex with DNA (colored by repeat) as a model of donor-acceptor fluorophore distances . (A) The distance from C30 in the first repeat (the site of labelling in NcTALE$_8$) to the 5' base of the sense strand (light grey) is 38.3Å; the distance to the 5' base of the antisense strand (dark grey) is 37.4Å. (B) The distance from C30 in the fourteenth repeat (the site of labelling in NcTALE$_{16}$) to the 5' base of the sense strand (light grey) is 72.9Å; the distance to the 5' base of the antisense strand (dark grey) is 25.1Å. Note that although there is likely to be some variation these distances since the DNAs used here are longer (15 and 23 bases) than the TALE arrays (8 and 16 repeats, each with a four-repeat N-capping domain), the differences in donor-acceptor distances for the 16 repeat construct (B) are likely to be robust to registry shifts of a few bases.

844

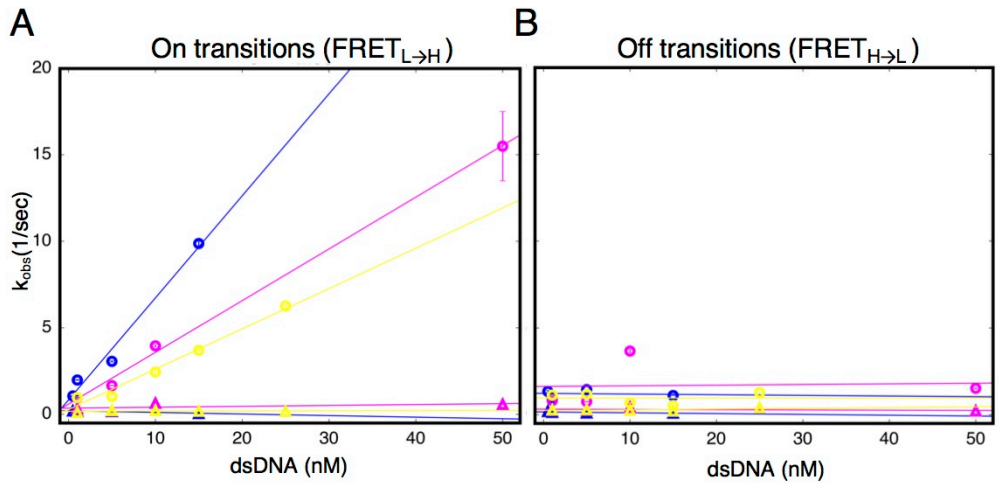

845

846 **Figure 6- figure supplement 3 1. Urea and destabilizing mutations decrease**

847 **apparent binding rate of cTALE$_8$.** (A) Apparent association rate constants as a

848 function of DNA concentration for an 8 repeat cTALE in 0 M urea (blue), 1 M urea

849 (pink), and with destabilizing point mutations (yellow; mutations substitute leucine at

850 position 1 in the fourth repeat with a glycine). The DNA concentration dependence is

851 strongest (steepest slope) in the absence of urea and destabilizing point substitutions

852 (circles). Rates in the slower phase (triangles) appear unaffected by urea or mutational

853 destabilization. (B) Apparent dissociation rate constants as a function of DNA

854 concentration (phase 1 shown in circles, and phase 2 shown in triangles). Rates in the

855 both phases appear unaffected by urea and mutational destabilization. Conditions: 200

856 mM KCl, 20 mM Tris pH 8.0.

857

Source Data

Figure 3- source data 1. List of values used to construct long time trajectories. Long time trajectories showing transitions between low- and high-FRET states (efficiencies of 0 and 0.45) for 1 nM dsDNA (source data 1A) and 15 nM dsDNA (source data 1B) depicted in Figure 3A-B.

Figure 3- source data 2. List of values used to construct CDFs. Cumulative distributions of low-FRET (source data 2A) and high-FRET (source data 2B) dwell times depicted in Figure 3C-D.